



Published in final edited form as:

*Cancer Immunol Res.* 2016 December ; 4(12): 1061–1071. doi:10.1158/2326-6066.CIR-16-0104.

## Established T-cell inflamed tumors rejected after adaptive resistance was reversed by combination STING activation and PD-1–pathway blockade

Ellen Moore<sup>1,\*</sup>, Paul E. Clavijo<sup>1,\*</sup>, Ruth Davis<sup>1</sup>, Harrison Cash<sup>1</sup>, Carter Van Waes<sup>1</sup>, Young Kim<sup>2</sup>, and Clint Allen<sup>1,2</sup>

<sup>1</sup>Head and Neck Surgery Branch, National Institute on Deafness and Other Communication Disorders, National Institutes of Health, Bethesda, MD

<sup>2</sup>Department of Otolaryngology-Head and Neck Surgery, Johns Hopkins School of Medicine, Baltimore, MD

### Abstract

Patients with head and neck squamous cell carcinoma harbor T-cell inflamed and non-T-cell inflamed tumors. Despite this, only 20% of patients respond to checkpoint inhibitor immunotherapy. Lack of induction of innate immunity through pattern-recognition receptors such as the stimulator of interferon (IFN) genes (STING) receptor may represent a significant barrier to the development of effective antitumor immunity. Here, we demonstrate robust control of a T-cell inflamed (MOC1), but not non-T-cell inflamed (MOC2), model of head and neck cancer by activation of the STING pathway with the synthetic cyclic dinucleotide R<sub>p</sub>,R<sub>p</sub> dithio-c-di-GMP. Rejection or durable tumor control of MOC1 tumors was dependent upon a functional STING receptor and CD8 T lymphocytes. STING activation resulted in increased tumor microenvironment type 1 and type 2 IFN and greater expression of PD-1–pathway components *in vivo*. Established MOC1 tumors were rejected and distant tumors abscopally controlled, after adaptive immune resistance had been reversed by the addition of PD-L1 mAb. These findings suggest that PD-1–pathway blockade may reverse adaptive immune resistance following cyclic dinucleotide treatment, enhancing both local and systemic antitumor immunity.

### Keywords

Antigenicity; immunogenicity; cyclic dinucleotide; STING; adaptive resistance

### Introduction

The stimulator of IFN genes (STING) receptor plays a critical role in Toll-like receptor–independent detection of pathogen-associated molecular patterns and type I IFN production in the induction of innate immunity (1,2). Detection of cytosolic DNA through cGAMP

**Corresponding author:** Clint Tanner Allen, MD, National Institutes of Health, 10 Center Drive, CRC 4-2740, Bethesda, MD 20892, P: 301-402-4216; F: 301-402-1140; clint.allen@nih.gov.

\*These authors contributed equally to this work

**Conflicts of interest:** None

synthase (cGAS) production of a noncanonical cyclic dinucleotide (CDN) and subsequent STING activation explains how innate immunity is initiated after tumor DNA is released into the “sterile” tumor microenvironment (3–5). Synthetic CDNs, designed to have improved *in vivo* stability and binding activity to both human and mouse STING, have been shown to have antitumor activity as adjuvants or monotherapies in a number of preclinical models (5,6).

Many head and neck squamous cell carcinomas (HNSCC) have high genetic alteration rates (7) and evidence of a T-cell inflamed phenotype (8,9) based on histologic and RNA-sequencing analysis (10). Blockade of programmed cell death (PD) receptor interactions with its ligands can induce durable antitumor responses, but only about 20% of head and neck cancer patients respond (11). However, upper aerodigestive tract cancers are often easily accessible for local injection, making them ideal candidates for treatment with intratumoral therapeutics. A phase I clinical trial investigating the safety of locally injected, single agent CDNs in the treatment of patients with recurrent head and neck squamous cell carcinoma (HNSCC) is underway. The potential of STING activation in combination with PD-based checkpoint inhibition in suitable syngeneic models of HNSCC has not been established.

Here, we demonstrate that local injection of the synthetic CDN R<sub>P</sub>,R<sub>P</sub> dithio c-di-GMP (R,R-CDG) potently induces either primary tumor growth control or rejection of established T-cell inflamed MOC1 tumors. Conversely, non-T-cell inflamed MOC2 tumors lack such responses. Within T-cell inflamed MOC1 tumors, R,R-CDG treatment led to induction of innate and antigen-specific adaptive immunity that was initially dependent upon STING and durably dependent upon CD8 T lymphocytes. Adaptive immune resistance (12) mediated by enhanced expression of tumor microenvironment PD-1 and its ligand PD-L1 after R,R-CDG treatment was reversed with PD-L1 mAb, further enhancing the rate of rejection of established MOC1 tumors and inducing potent systemic antitumor immunity that led to abscopal control of distant tumors. Although others have demonstrated that adaptive immune resistance and tumor rejection can be reversed by checkpoint inhibition in tumors treated with STING agonist–formulated cancer vaccines (6), this study demonstrates such effects with synthetic CDN alone. These findings indicate that adaptive immune resistance following CDN alone can be reversed with PD-1-pathway blockade, with resulting enhanced local and systemic antitumor immunity.

## Materials and Methods

### Irradiated whole cell vaccination

Murine oral cancer (MOC) 1 and 2 cells were provided by Dr. R. Uppaluri (Washington University School of Medicine) in 2014 (13), maintained in culture as previously described for no more than 20 passages (14), authenticated by exome sequencing by others (15) and by cytokeratin immunofluorescence by our laboratory, and tested monthly for mycoplasma. For *in vitro* experiments, cells were harvested with TrypLE Select (ThermoFisher) at 80% confluence and viability was determined via propidium iodide exclusion. MOC cells were irradiated to 100 Gy with a <sup>137</sup>Cs source irradiator (Gammacell-1000). Irradiated MOC1 or 2 cells were injected subcutaneously (subq) into the flanks of 8-week female wild-type

C57BL/6 (WT B6, Charles River Laboratories) mice suspended in 30% complete Freund's Adjuvant (% vol). Four weeks after vaccination, naïve and vaccinated mice were challenged with untreated MOC1 ( $2 \times 10^6$ ) or MOC2 ( $1 \times 10^5$ ) cells and were evaluated for tumor engraftment. All experiments were approved by the NIDCD Animal Care and Use Committee (ASP #1364-14).

### **In vitro treatments**

MOC1 and 2 cells were plated, allowed to reach 75% confluence, and treated with either R,R-CDG (Aduro Pharmaceuticals, synthesis described by Baird et al. (16)), recombinant murine IFN $\beta$ , (Biolegend) or control (1 $\times$  PBS).

### **In vivo treatments**

MOC1 ( $2 \times 10^6$ ) or MOC2 ( $1 \times 10^5$ ) cells were injected subq into the flanks of WT B6 mice. Bilateral tumors were implanted for abscopal experiments. All tumors were engrafted to at least 0.1 cm<sup>3</sup> (6–7 mm diameter) before treatment. Mice were weighed and tumors were measured three times weekly. Intratumoral injections of R,R-CDG in HBSS (100  $\mu$ L volume) were directed at the deep aspect of the tumor. Control mice received HBSS alone. PD-L1 mAb (clone 10F.9G2, rat IgG2b, BioXCell) or rat IgG isotype control antibody treatments were performed via intraperitoneal (IP) injection (200  $\mu$ g/injection). In some experiments, C57BL/6J-*Tmem173<sup>gt</sup>*/J STING-deficient mice (Jackson Laboratories) were used. In other experiments, cellular or cytokine depletions were performed via IP injection of CD8 (clone YTS169.4), IFN $\gamma$  (clone XMG1.2) or TNF $\alpha$  (clone XT3.11) mAbs (200  $\mu$ g/injection; BioXCell).

### **In vitro cell viability**

Viability of MOC cells was measured via XTT (Trevigen) assay per manufacturer protocol.

### **RT-PCR**

Tumor homogenates were generated from snap frozen tissue using the Tissue Lysate II per manufacturer protocol. RNA was extracted from MOC cells or tissue homogenates using the RNEasy Mini Kit (Qiagen) or the PicoPure RNA Isolation Kit (ThermoFisher) following manufacturer protocol. cDNA was synthesized using high capacity reverse transcription. Gene expression was determined relative to GAPDH at baseline and following treatments using single tube primers (Life Technologies) on a Vii7 qPCR analyzer (Applied Biosystems).

### **Flow cytometry**

MOC cells were harvested and non-specific binding was blocked with anti-CD16/32 antibodies (Biolegend) prior to staining. Tissues were prepared into single-cell suspensions as previously described (14), followed by anti-CD16/32 antibody staining. Cell surface staining was performed using fluorophore conjugated anti-mouse CD45.2 clone 104, CD3 clone 145-2C11, CD4 clone GK1.5, CD8 clone 53-6.7, NK1.1 clone PK136, CD31 clone 390, PD-L1 clone 10F.9G2, H2-K<sup>b</sup> clone AF6-88.5, CD107a clone 1D4B, CD69 clone H1.2F3, PD-1 clone RMP1-30, CD11b clone M1/70, CD11c clone N418, CD80 clone

16-10A1, and CD86 clone GL-1 antibodies from Biolegend, 41BB clone 17B5 and OX40 clone OX-86 from eBioscience, and CD8 clone KT15 from MBL (Woburn, MA). H2Kb:KSPWF<sub>604-611</sub>TTL tetramer was purchased from MBL. Dead cells were excluded via 7AAD negativity. Isotype control antibodies and a “fluorescence minus one” method of antibody combination were used for specific staining validation. Data was acquired on a FACSCanto using FACSDiva software (BD Biosciences) and analyzed on FlowJo software vX10.0.7r2.

### Cell sorting

Single cell suspensions were generated from spleens and lymph nodes from WT B6 mice. Cells were stained and sorted on an autoMACS magnetic sorter (Miltenyi Biotec) using CD19 positive selection (B lymphocyte), pan T-cell negative selection (T lymphocyte), NK cell negative selection (NK cells), pan DC positive selection (DC cells) and CD11b positive selection (myeloid cell) kits from Miltenyi. Purity of each cell population was > 90% as assessed by flow cytometry.

### Immunofluorescence

Tumor tissue was embedded in optimum cutting temperature media. Sections (6 μm) were fixed with methanol, washed, and nonspecific binding was blocked with a solution of 3% BSA and 0.1% tween 20 in 1×PBS. AF594-conjugated PD-L1 (clone MIH6, Abcam) or isotype control antibody was incubated overnight at 4°C in a humidified chamber. Following washes, slides were counterstained with DAPI and mounted for analysis on a LSM 780 confocal microscope (Zeiss). Photomicrographs were analyzed using Zen 2012 SP1 software.

### *In vivo* cytotoxic T-lymphocyte assay

Splenocytes were harvested from naïve B6 mice and labeled with 2.5 or 0.25 μM CFSE. High CFSE labeled cells were pulsed with 10 μg/mL of p15E<sub>604-611</sub> (KSPWF<sub>604-611</sub>TTL) or control OVA<sub>257-264</sub> (SIINFEKL) peptide for one hour. Cells were washed, mixed and adoptively transferred into naïve, control or treated MOC tumor-bearing mice. Four hours later, splenocytes were harvested and flow cytometry was used to determine the ratio of CFSE high to CFSE low cells. Antigen-specific cell killing was determined as:  $1 - (r_{\text{naïve}} / r_{\text{vaccinated}}) \times 100$ , where  $r = (\% \text{ CFSE low cells}) / (\% \text{ CFSE high cells})$ .

### Statistical analysis

Tests of significance between pairs of data are reported as *P* values, derived using a Fisher exact test or student *t*-test with a two-tailed distribution and calculated at 95% confidence. Comparison of multiple sets of data was achieved with one or two-way analysis of variance (ANOVA). Kaplan-Meier curves were compared using the log-rank/Mantel Cox test. Error bars reflect standard error of measurement (SEM). Analysis was performed using GraphPad Prism v6.

## Results

### Immunologic memory induced by whole-cell vaccination with MOC1, but not MOC2

Patients with HNSCCs demonstrate significant heterogeneity in tumor T-cell inflamed status. Previous work has demonstrated the T-cell inflamed status of MOC1 tumors and non-T-cell inflamed status of MOC2 tumors (17,18). We performed whole tumor cell vaccination experiments to explore the ability of MOC1 and MOC2 cells to induce immunologic memory and to further validate their use in modeling both T-cell inflamed and non-T-cell inflamed HNSCCs. WT B6 mice vaccinated with irradiated MOC1 efficiently resisted engraftment when challenged with MOC1, but not MOC2, cells (Fig. 1A). This suggests that there are tumor rejection antigens present on MOC1 cells capable of inducing immunologic memory. Either no antigens are shared between MOC1 and MOC2 or MOC2 cells possess an intrinsic insensitivity to T cell-mediated cell killing. In support of this, MOC2 tumors readily engrafted following MOC2 cell challenge after vaccination with irradiated MOC2 cells (Fig. 1B). Thus the ability of MOC1 and MOC2 cells to induce immunologic memory is consistent with their T-cell inflamed status and suggest that these two cancer cell lines can serve as models of human HNSCC with variable T-cell inflamed status.

### CDN induces rejection of a subset of established MOC1, but not MOC2, tumors

We treated established (at least 0.1 cm<sup>3</sup>, or 6–7 mm diameter) MOC1 and MOC2 tumors, growing in WT B6 mice, with three intratumoral injections of R,R-CDG. This treatment resulted in complete tumor rejection in 5/10 established MOC1 tumors, and significant growth inhibition in the remaining tumors, leading to significantly prolonged survival ( $P < 0.001$ ) in MOC1 tumor-bearing mice treated with CDN compared to control (Fig. 2A). Mice that rejected established MOC1 tumors were challenged with MOC1 cells, which resulted in no tumor formation, indicating the formation of immunologic memory (Fig. 2B). Similar to the vaccination experiments, R,R-CDG-treated mice that rejected established MOC1 tumors and subsequent MOC1 challenge readily formed tumors when challenged with MOC2 transplantation. Conversely, R,R-CDG treatment of established MOC2 tumors slightly delayed primary tumor growth in a subset of tumors, but did not result in significant prolongation of survival (Fig. 2C). Mice that rejected established MOC1 tumors developed physical findings consistent with an immune-mediated mechanism, including vitiligo and hair loss at the former tumor site (**example pictured in** Fig. 2D). These data indicate that STING agonists are able to induce antitumor immunity in T-cell inflamed but not non-T-cell inflamed tumors.

### CDN-induced type I IFN from immune cells enhanced MOC cell immunogenicity *in vitro*

We next assessed whether R,R-CDG is directly cytotoxic to MOC cells. Results from XTT viability assays suggest that the observed *in vivo* effect is not due to direct cytotoxicity as exposure of MOC cells to R,R-CDG at doses up to 20  $\mu$ M induced no reduction in cell viability (Fig. 3A). Given that STING is known to serve as the cognate CDN receptor(5), we determined STING expression levels in MOC and sorted immune cell subsets. All immune cell subsets expressed STING at significantly higher levels than either MOC1 or MOC2, with myeloid cell subsets (total CD11b<sup>+</sup> myeloid and CD11c<sup>+</sup> DCs) demonstrating the highest relative STING expression (Fig. 3B). Functionally, STING expression correlated

with type I interferon production upon exposure to R,R-CDG (Fig. 3C), with dose-dependent induction of IFN $\beta$  expression in immune subsets but not MOC cells. IFN $\beta$ , but not R,R-CDG, was able to enhance MOC cell expression of genes encoding for antigen processing machinery components (Fig. 3D), as well as cell surface expression of calreticulin, MHC class I and II, and PD-L1 (Fig. 3E). Taken together, these data demonstrate that R,R-CDG exposure leads to type I IFN production by immune cells with subsequent enhancement of MOC cell immunogenicity. This data also suggests that the lack of MOC2 response to CDN is not due to an intrinsic insensitivity to interferon.

### **CDN-treated MOC1-bearing mice have increased type I IFN and better adaptive immunity**

We analyzed multiple immune correlates in control and R,R-CDG treated MOC1 tumors and tumor-draining lymph nodes (DLNs). Using flow cytometry, we observed enhanced MOC1 tumor and infiltrating immune cell specific PD-L1 and tumor cell MHC class I expression (H2-K<sup>b</sup>) following treatment (Fig. 4A, validated with immunofluorescence in Fig. 4B). CD8<sup>+</sup> dendritic cells (DCs) are critical for cross presentation of tumor antigen to activate adaptive immunity (19,20). Fig. 4C demonstrates enhanced accumulation of total DLN DCs and accumulation and activation (CD80/86) of CD8<sup>+</sup> DLN DCs following treatment. Quantification of tumor infiltrating lymphocytes (TIL) revealed substantially enhanced accumulation and activation of both total (PD-1, CD69, 41BB exhaustion/activation markers) and p15E<sub>604-611</sub> antigen-specific (CD107a activation marker) CD8 TIL into MOC1 tumors following treatment (Fig. 4D). Accumulation and activation (PD-1, OX40 exhaustion/activation markers) of CD4 TIL was also increased after treatment (Supplementary Fig. S1A). Tumor NK cell infiltration was not increased, but activation of infiltrating NK cells was modestly enhanced after treatment (Supplementary Fig. S1B). Representative flow cytometry dot plots for select cellular subsets are shown in Supplementary Fig. S2. Concentrations of IFN $\alpha$  and IFN $\beta$  and effector cytokines IFN $\gamma$  and TNF $\alpha$  from whole tumor or DLN tissue homogenates were determined (Fig. 4E and F). CDN-treated MOC1 tumors had substantially increased IFN $\beta$ , the DLNs had modestly increased IFN $\beta$ , and effector cytokines were significantly elevated in both. Conversely, treatment of unresponsive MOC2 tumors with R,R-CDG appeared to increase tumor IFN $\beta$  and the accumulation of DLN DCs, but not TIL or PD-L1 expression within the tumor microenvironment (Supplementary Fig. S3). Cumulatively, these data provide correlative support for R,R-CDG-induced activation of innate immunity with subsequent development of antigen-specific adaptive immunity within MOC1, but not MOC2, tumors.

### **STING and CD8 TIL are required for R,R-CDG-induced MOC1 tumor control *in vivo***

We treated established MOC1 tumors in STING-deficient B6 mice in parallel with WT B6 mice (Fig. 5A). Not only did MOC1 primary tumors grow more rapidly in STING-deficient mice, they were completely unresponsive to intratumoral R,R-CDG treatments. We next performed antibody-based cellular and cytokine depletions in MOC1 tumor-bearing WT B6 mice. Depletion of CD8 and IFN $\gamma$ , but not TNF $\alpha$ , abrogated R,R-CDG-induced MOC1 tumor rejection and growth control. Mice with MOC1 tumors and with CD8 or IFN $\gamma$  depletion initially responded to R,R-CDG, but durable responses were lost: tumor growth rebounded approximately one week after completion of treatment. Flow cytometric analysis of MOC1 tumor tissue from STING-deficient mice revealed near-complete loss of CD8 and

CD4 TIL accumulation that was not enhanced with R,R-CDG treatment (Fig. 5B). Analysis of STING-deficient tumor tissues revealed abrogation of R,R-CDG-induced MOC1 tumor cell surface PD-L1 and MHC class I expression and loss of accumulation of type I IFN and effector cytokines in the tumor microenvironment after treatment (Fig. 5C). Baseline tumor IFN $\gamma$  expression was substantially reduced in STING-deficient mice compared to WT B6 mice. Mechanistically, these data validate the role of STING signaling in the baseline induction of MOC1 antitumor immunity, and provide strong evidence that R,R-CDG induces production of STING-dependent type I IFN within the MOC1 tumor microenvironment that subsequently leads to the development of CD8<sup>+</sup> T cell-dependent adaptive antitumor immunity.

### Combination CDN and PD-L1 mAb leads to enhanced rejection of MOC1 tumors

Given the enhanced tumor and immune cell expression of PD-L1 and PD-1 expression on CD8<sup>+</sup> and CD4<sup>+</sup> TILs in MOC1 tumors *in vivo* after R,R-CDG treatment, we hypothesized that combination R,R-CDG and PD-L1 mAb treatment would further enhance rejection rates of MOC1 tumors. We treated established MOC1 tumors with R,R-CDG and PD-L1 mAb, alone or in combination, and measured primary tumor growth and time to 750 mm<sup>3</sup> as a statistical readout (Fig. 6A). Treatment with PD-L1 mAb alone delayed primary tumor growth, but tumors eventually rebounded and no tumors were rejected, consistent with previous experiments (17) (Fig. 6B). Following R,R-CDG treatment alone, 5/10 tumors were rejected and 4/5 remaining primary tumors grew at a reduced rate. However, the combination of R,R-CDG and PD-L1 mAb induced rejection of 90% of MOC1 tumors, with the remaining tumor displaying reduced growth. This combination antitumor effect was significantly more robust ( $P=0.041$ , log-rank/Mantel Cox analysis for time to 750 mm<sup>3</sup>) than R,R-CDG treatment alone (Fig. 6C). Thus, the addition of PD-L1 mAb to R,R-CDG treatment appears to reverse adaptive immune resistance and enhance rates of MOC1 tumor rejection.

### Combination treatment induces protective memory and abscopal tumor control

To validate that R,R-CDG and anti-PD-L1 mAb treatments led to the development of systemic antitumor immunity, we utilized an *in vivo* CTL assay (Fig. 7A). Selective killing of adoptively transferred splenocytes presenting p15E<sub>604-611</sub> peptide as a model antigen was significantly increased in mice treated with the combination therapy compared to control or either therapy alone. Specificity of the *in vivo* CTL assay was validated with control (SIINFEKL) peptide-pulsed, adoptively, transferred splenocytes in mice vaccinated with p15E peptide (Supplementary Fig. S4). Mice that rejected MOC1 tumor following combination treatment resisted challenge with MOC1 cells (Fig. 7B). To further establish the development of systemic antigen-specific immunity, we performed abscopal experiments (Fig. 7C). Treatment of right flank tumors with R,R-CDG in the presence of systemic PD-L1 mAb, but not with R,R-CDG or PD-L1 mAb alone, induced near-complete tumor control of contralateral untreated tumors. Thus, reversal of adaptive immune resistance by adding PD-L1 mAb to R,R-CDG results in systemic antigen-specific antitumor immunity that can control distant deposits of tumor.

## Discussion

Previous work has established the role of STING pathway activation as an adjuvant therapy for antitumor peptide and GM-secreting whole tumor cell vaccines (6,21,22). Our work reported here demonstrates significant tumor control can be had through STING pathway activation as a monotherapy in a carcinogen-induced model of HNSCC, and that adaptive immune resistance can be reversed, with complete tumor rejection and abscopal control of distant tumors, by treatment with the combination of nonformulated R,R-CDG and checkpoint inhibition. Significant primary tumor growth control and consistent tumor rejection rates of about 50% were achieved with the synthetic noncanonical CDN R,R-CDG, shown to be more potent than natural CDN compounds or other synthetic formulations (5,6). We demonstrated evidence of adaptive immune resistance (12) following R,R-CDG treatment with increased tumor and immune cell PD-L1, and TIL PD-1, expression. Combining STING-pathway activation with PD-L1 mAb led to consistent rejection of 90% of established MOC1 tumors, with the development of more robust antigen-specific immunologic memory and abscopal control of distant, untreated tumors. Enhanced antitumor immunity with vaccine-formulated or other CDNs and checkpoint inhibitors has also been demonstrated in models of melanoma and colon cancer (6,23). Mechanistically we demonstrated early STING and late CD8 dependent tumor control, with production of type I IFN appearing to come primarily from infiltrating host cells and not tumor cells, consistent with other studies (4,16,24,25).

Our use of both T-cell inflamed (MOC1) and non-T-cell inflamed tumors (MOC2) allows us to model both immunogenic and poorly immunogenic HNSCCs. Rejection of a subset of T-cell inflamed MOC1 tumors with R,R-CDG treatment alone, which are relatively insensitive to PD-based checkpoint inhibition alone, suggests that lack of innate immune activation may limit responses achievable with PD blockade in some tumors. Lack of response to R,R-CDG in non-T-cell inflamed MOC2 tumors suggests that STING-dependent induction of antitumor immunity is dependent upon the baseline T-cell inflamed status of the tumor and likely the presence of tumor rejection antigen(s). Treatment of MOC2 tumors with R,R-CDG induced type I IFN within the tumor microenvironment and increased DCs within the DLN, but not accumulation of CD8<sup>+</sup> TILs, suggesting that the lack of tumor control observed with this model was due to an intrinsic insensitivity of MOC2 to immune control and not due to alteration of innate immune cells within the MOC2 tumor microenvironment leading to insensitivity to CDN. Poor antigenicity of MOC2 or an intrinsic insensitivity of MOC2 to T-lymphocyte killing could explain these findings. Lemos et al. have shown the promotion of Lewis lung carcinoma tumor growth that was secondary to IDO production following STING activation (26). These results were reversed with the introduction of a tumor rejection antigen into the cancer cells, providing evidence that STING activation within the tumor microenvironment can have dramatically different results based on tumor cell antigenicity. Previous work by others has established that chronic type I IFN signaling through STING can promote carcinogen-induced tumorigenesis (27) and lead to induction of T-lymphocyte tolerance through IDO production (28,29). How STING signaling, in the presence or absence of tumor rejection antigen, serves as a switch between protective type I



IFN-dependent immunity and tumor-promoting inflammation needs clarification and has significant implications for the clinical translation of STING agonists.

Antigenic heterogeneity of tumor rejection antigens may contribute to variability in responsiveness to STING activation. Since we have not identified all tumor rejection antigens present in MOC1, our use of p15E as a model antigen makes our understanding of antigen spread and TIL response to neoantigens incomplete. However, the addition of PD-L1 mAb largely rescued MOC1 tumors from adaptive immune resistance following CDN treatment, which points to the importance of adaptive immunity in this treatment approach. Additionally, our analysis of immune correlative alterations following R-R-CDG treatment was incomplete. Although we demonstrated increased PD-L1 expression on both tumor and infiltrating immune cells within the MOC1 tumor microenvironment, we did not mechanistically explore which immune cells dominantly express PD-L1 for ligation with PD-1 on CD8<sup>+</sup> TILs. It is possible that certain immune cell subsets, such as myeloid-derived suppressor cells or myeloid dendritic cells, dominantly contribute PD-L1 at baseline or in response to IFN (30,31). Further, early responses to CDN may be mediated through vascular disruption and tumor necrosis (16,32) and these parameters were not explored in our studies. Our finding that *early* growth control in MOC1 tumors following R,R-CDG treatment was abrogated in STING-deficient mice, but minimally altered by CD8<sup>+</sup> T cells or IFN $\gamma$ , suggests mechanisms independent of adaptive immunity but still dependent on host cells, which may include myeloid or NK cell activity (16,33). This early necrotic response following STING activation may be *required* for efficient induction of antitumor immunity, as pro-apoptotic caspases suppress type I IFN production following STING detection of cytosolic DNA (34). Further exploration of these early responses will be important to understand how STING activation can be optimally utilized and possibly sequenced with other anticancer treatments to induce antitumor immunity.

In summary, we demonstrated robust induction of innate and adaptive antitumor immunity following STING activation with a synthetic CDN compound, which led to rejection of a subset of established T-cell inflamed MOC1 tumors. This finding could not be reproduced in non-T-cell inflamed MOC2 tumors. Antitumor immunity was dependent upon a functional STING receptor and durable tumor control was dependent upon CD8<sup>+</sup> T lymphocytes. Reversal of adaptive immune resistance with combination STING activation and PD-L1 mAb led to rejection of 90% of established MOC1 tumors and control of distant, untreated tumors, indicating the development of systemic, antigen-specific antitumor immunity. The clinical safety of locally injected STING agonists is being tested in phase I studies currently underway. This preclinical data may serve as a rationale for combining CDN with checkpoint inhibition to reverse adaptive immune resistance.

## Supplementary Material

Refer to Web version on PubMed Central for supplementary material.

## Acknowledgments

The authors thank James Hodge and Ravindra Uppaluri for their critical review of this manuscript.

**Financial support:** This work was supported by the Intramural Research Program of the NIH, NIDCD, project number ZIA-DC000087. RD was supported through the National Institutes of Health (NIH) Medical Research Scholars Program, a public-private partnership supported jointly by the NIH and generous contributions to the Foundation for the NIH from Pfizer Inc, The Doris Duke Charitable Foundation, The Newport Foundation, The American Association for Dental Research, The Howard Hughes Medical Institute, and the Colgate-Palmolive Company, as well as other private donors. CA received further support through the American Academy of Otolaryngology/American Head and Neck Society Duane Sewell Young Investigators Award.

## References

1. Ishikawa H, Barber GN. STING is an endoplasmic reticulum adaptor that facilitates innate immune signalling. *Nature*. 2008; 455:674–678. [PubMed: 18724357]
2. Ishikawa H, Ma Z, Barber GN. STING regulates intracellular DNA-mediated, type I interferon-dependent innate immunity. *Nature*. 2009; 461:788–792. [PubMed: 19776740]
3. Diner EJ, Burdette DL, Wilson SC, Monroe KM, Kellenberger CA, Hyodo M, et al. The innate immune DNA sensor cGAS produces a noncanonical cyclic dinucleotide that activates human STING. *Cell Rep*. 2013; 3:1355–1361. [PubMed: 23707065]
4. Klarquist J, Hennies CM, Lehn MA, Reboulet RA, Feau S, Janssen EM. STING-mediated DNA sensing promotes antitumor and autoimmune responses to dying cells. *J Immunol*. 2014; 193(12): 6124–6134. [PubMed: 25385820]
5. Corrales L, Glickman LH, McWhirter SM, Kanne DB, Sivick KE, Katibah GE, et al. Direct Activation of STING in the Tumor Microenvironment Leads to Potent and Systemic Tumor Regression and Immunity. *Cell Rep*. 2015; 11:1018–1030. [PubMed: 25959818]
6. Fu J, Kanne DB, Leong M, Glickman LH, McWhirter SM, Lemmens E, et al. STING agonist formulated cancer vaccines can cure established tumors resistant to PD-1 blockade. *Sci Transl Med*. 2015; 7:283–294.
7. Cancer Genome Atlas N. Comprehensive genomic characterization of head and neck squamous cell carcinomas. *Nature*. 2015; 517:576–582. [PubMed: 25631445]
8. Woo SR, Corrales L, Gajewski TF. The STING pathway and the T cell-inflamed tumor microenvironment. *Trends Immunol*. 2015; 36:250–256. [PubMed: 25758021]
9. Gajewski TF, Schreiber H, Fu YX. Innate and adaptive immune cells in the tumor microenvironment. *Nat Immunol*. 2013; 14:1014–1022. [PubMed: 24048123]
10. Keck MK, Zuo Z, Khattri A, Stricker TP, Brown CD, Imanguli M, et al. Integrative analysis of head and neck cancer identifies two biologically distinct HPV and three non-HPV subtypes. *Clin Cancer Res*. 2015; 21:870–881. [PubMed: 25492084]
11. Seiwert TY, Burtneß B, Mehra R, Weiss J, Berger R, Eder JP, et al. Safety and clinical activity of pembrolizumab for treatment of recurrent or metastatic squamous cell carcinoma of the head and neck (KEYNOTE-012): an open-label, multicentre, phase 1b trial. *Lancet Oncol*. 2016; 17:956–965. [PubMed: 27247226]
12. Taube JM, Klein A, Brahmer JR, Xu H, Pan X, Kim JH, et al. Association of PD-1, PD-1 ligands, and other features of the tumor immune microenvironment with response to anti-PD-1 therapy. *Clin Cancer Res*. 2014; 20:5064–5074. [PubMed: 24714771]
13. Judd NP, Winkler AE, Murillo-Sauca O, Brotman JJ, Law JH, Lewis JS Jr, et al. ERK1/2 regulation of CD44 modulates oral cancer aggressiveness. *Cancer Res*. 2012; 72:365–374. [PubMed: 22086849]
14. Cash H, Shah S, Moore E, Caruso A, Uppaluri R, Van Waes C, et al. mTOR and MEK1/2 inhibition differentially modulate tumor growth and the immune microenvironment in syngeneic models of oral cavity cancer. *Oncotarget*. 2015; 6:36400–36417. [PubMed: 26506415]
15. Onken MD, Winkler AE, Kanchi KL, Chalivendra V, Law JH, Rickert CG, et al. A surprising cross-species conservation in the genomic landscape of mouse and human oral cancer identifies a transcriptional signature predicting metastatic disease. *Clin Cancer Res*. 2014; 20:2873–2884. [PubMed: 24668645]
16. Baird JR, Friedman D, Cottam B, Dubensky TW Jr, Kanne DB, Bambina S, et al. Radiotherapy Combined with Novel STING-Targeting Oligonucleotides Results in Regression of Established Tumors. *Cancer Res*. 2016; 76:50–61. [PubMed: 26567136]

17. Moore EC, Cash HA, Caruso AM, Uppaluri R, Hodge JW, Van Waes C, et al. Enhanced Tumor Control with Combination mTOR and PD-L1 Inhibition in Syngeneic Oral Cavity Cancers. *Cancer Immunol Res.* 2016; 4:611–620. [PubMed: 27076449]
18. Shah S, Caruso A, Cash H, Waes CV, Allen CT. Pools of programmed death-ligand within the oral cavity tumor microenvironment: Variable alteration by targeted therapies. *Head Neck.* 2016; 38:1176–1186. [PubMed: 27061215]
19. Diamond MS, Kinder M, Matsushita H, Mashayekhi M, Dunn GP, Archambault JM, et al. Type I interferon is selectively required by dendritic cells for immune rejection of tumors. *J Exp Med.* 2011; 208:1989–2003. [PubMed: 21930769]
20. Fuertes MB, Kacha AK, Kline J, Woo SR, Kranz DM, Murphy KM, et al. Host type I IFN signals are required for antitumor CD8<sup>+</sup> T cell responses through CD8 $\alpha$ <sup>+</sup> dendritic cells. *J Exp Med.* 2011; 208:2005–2016. [PubMed: 21930765]
21. Wang Z, Celis E. STING activator c-di-GMP enhances the anti-tumor effects of peptide vaccines in melanoma-bearing mice. *Cancer Immunol Immunother.* 2015; 64:1057–1066. [PubMed: 25986168]
22. Chandra D, Quispe-Tintaya W, Jahangir A, Asafu-Adjei D, Ramos I, Sintim HO, et al. STING ligand c-di-GMP improves cancer vaccination against metastatic breast cancer. *Cancer Immunol Res.* 2014; 2:901–910. [PubMed: 24913717]
23. Demaria O, De Gassart A, Coso S, Gestermann N, Di Domizio J, Flatz L, et al. STING activation of tumor endothelial cells initiates spontaneous and therapeutic antitumor immunity. *Proc Natl Acad Sci U S A.* 2015; 112:15408–15413. [PubMed: 26607445]
24. Woo SR, Fuertes MB, Corrales L, Spranger S, Furdyna MJ, Leung MY, et al. STING-dependent cytosolic DNA sensing mediates innate immune recognition of immunogenic tumors. *Immunity.* 2014; 41:830–842. [PubMed: 25517615]
25. Thomas GR, Chen Z, Enamorado I, Bancroft C, Van Waes C. IL-12- and IL-2-induced tumor regression in a new murine model of oral squamous-cell carcinoma is promoted by expression of the CD80 co-stimulatory molecule and interferon-gamma. *Int J Cancer.* 2000; 86:368–374. [PubMed: 10760825]
26. Lemos H, Mohamed E, Huang L, Ou R, Pacholczyk G, Arbab AS, et al. STING Promotes the Growth of Tumors Characterized by Low Antigenicity via IDO Activation. *Cancer Res.* 2016; 76:2076–2081. [PubMed: 26964621]
27. Ahn J, Xia T, Konno H, Konno K, Ruiz P, Barber GN. Inflammation-driven carcinogenesis is mediated through STING. *Nat Commun.* 2014; 5:5166–5175. [PubMed: 25300616]
28. Abe T, Harashima A, Xia T, Konno H, Konno K, Morales A, et al. STING recognition of cytoplasmic DNA instigates cellular defense. *Mol Cell.* 2013; 50:5–15. [PubMed: 23478444]
29. Huang L, Li L, Lemos H, Chandler PR, Pacholczyk G, Baban B, et al. Cutting edge: DNA sensing via the STING adaptor in myeloid dendritic cells induces potent tolerogenic responses. *J Immunol.* 2013; 191:3509–3513. [PubMed: 23986532]
30. Curiel TJ, Wei S, Dong H, Alvarez X, Cheng P, Mottram P, et al. Blockade of B7-H1 improves myeloid dendritic cell-mediated antitumor immunity. *Nat Med.* 2003; 9:562–567. [PubMed: 12704383]
31. Noman MZ, Desantis G, Janji B, Hasmim M, Karray S, Dessen P, et al. PD-L1 is a novel direct target of HIF-1 $\alpha$ , and its blockade under hypoxia enhanced MDSC-mediated T cell activation. *J Exp Med.* 2014; 211:781–790. [PubMed: 24778419]
32. Downey CM, Aghaei M, Schwendener RA, Jirik FR. DMXAA causes tumor site-specific vascular disruption in murine non-small cell lung cancer, and like the endogenous non-canonical cyclic dinucleotide STING agonist, 2'3'-cGAMP, induces M2 macrophage repolarization. *PLoS One.* 2014; 9:e99988. [PubMed: 24940883]
33. Lam AR, Le Bert N, Ho SS, Shen YJ, Tang ML, Xiong GM, et al. RAE1 ligands for the NKG2D receptor are regulated by STING-dependent DNA sensor pathways in lymphoma. *Cancer Res.* 2014; 74:2193–2203. [PubMed: 24590060]
34. White MJ, McArthur K, Metcalf D, Lane RM, Cambier JC, Herold MJ, et al. Apoptotic caspases suppress mtDNA-induced STING-mediated type I IFN production. *Cell.* 2014; 159:1549–1562. [PubMed: 25525874]

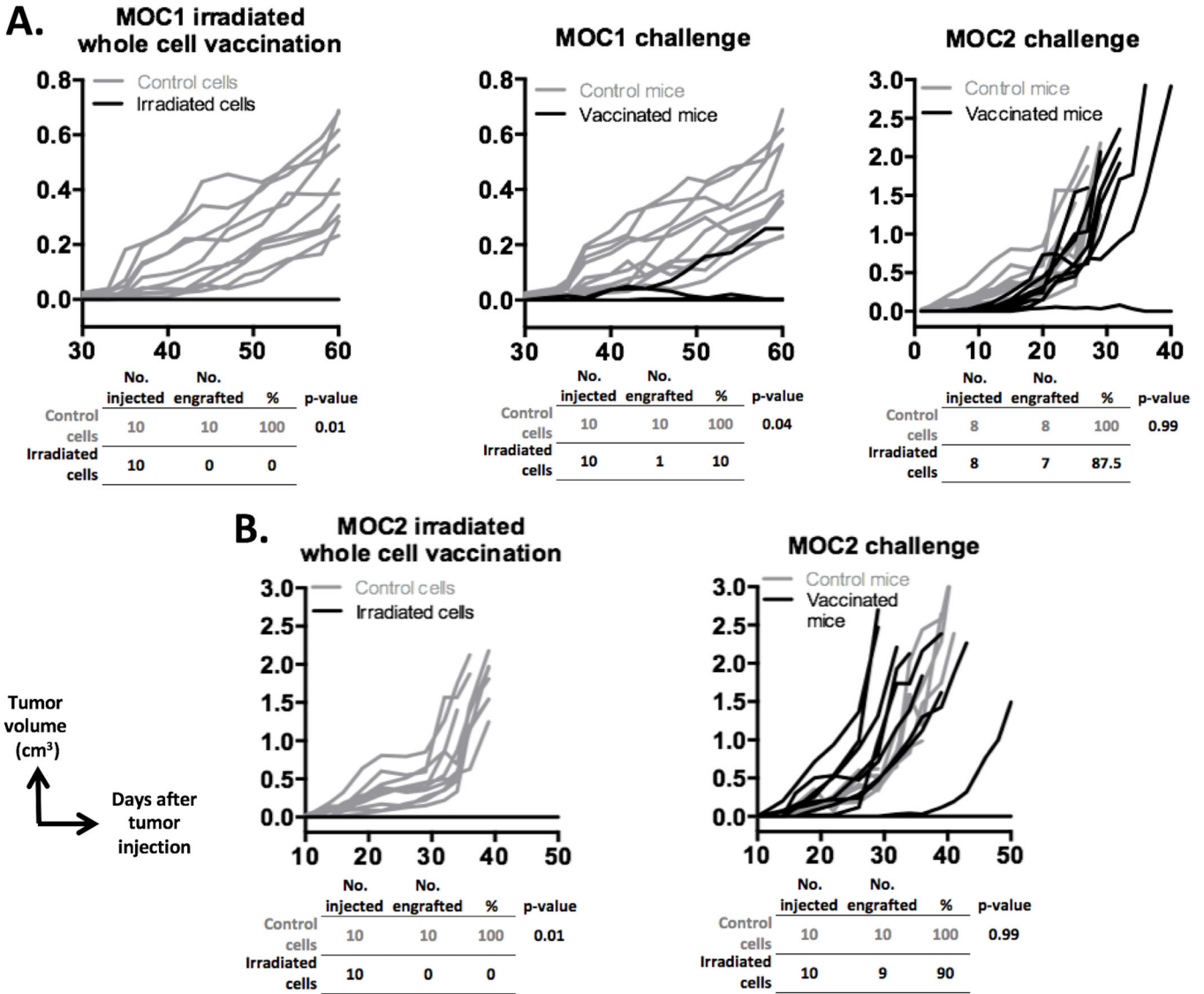


**Figure 1. Irradiated whole cell vaccination with MOC1, but not MOC2, induces immunologic memory**

**A**,  $1 \times 10^6$  untreated or irradiated MOC1 cells were injected into WT B6 mice in complete Freund's Adjuvant (left plot,  $n = 10$  mice/group). Four weeks later,  $2 \times 10^6$  untreated MOC1 cells were injected into separate cohorts of naïve and vaccinated mice (middle plot). Vaccinated mice that did not engraft tumors following MOC1 challenge (9 of 10 challenged mice) were re-challenged with  $1 \times 10^5$  MOC2 cells (right plot). **B**,  $1 \times 10^5$  untreated or  $1 \times 10^6$  irradiated MOC2 cells were injected into WT B6 mice (left plot). Vaccinated or control WT B6 mice were then challenged with  $1 \times 10^5$  MOC2 cells (right plot). Rates of engraftment are shown below each plot. *P* values were calculated using the Fisher exact test. Growth curves shown are representative of two series of independent experiments with similar results.

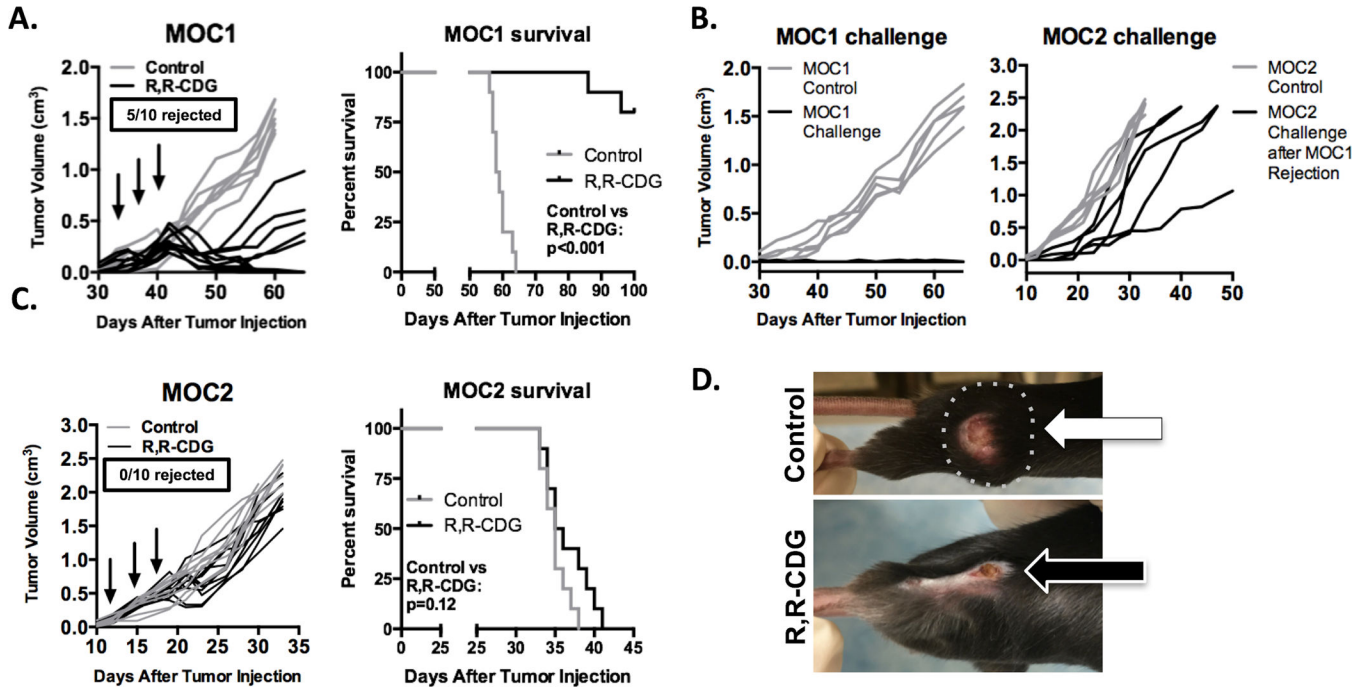


**Figure 2. Subsets of established MOC1, but not MOC2, tumors reject following CDN monotherapy**

**A**, established MOC1 tumors (0.1 cm<sup>3</sup> volume average) were treated with intratumoral injection of R,R-CDG (15 µg/injection q 3 days × 3, n = 10 mice/group, left panel). Black arrows indicate R,R-CDG injections. Mice were followed for 100 days and survival analyzed (right panel, log-rank/Mantel Cox test). End-point criteria for survival was tumor diameter of 2 cm. **B**, mice that rejected MOC1 tumors following treatment (5/10 mice) were challenged with 2 × 10<sup>6</sup> MOC1 cells 30 days after tumor rejection (left panel). Thirty days after this MOC1 challenge, these same mice were challenged with MOC2 (right panel). **C**, treatment of established MOC2 tumors with intratumoral R,R-CDG (left panel, n = 10 mice/group) and corresponding survival analysis (right panel). **D**, photographs of control (top, broken line is palpable tumor) and R,R-CDG treated (bottom) MOC1 tumor-bearing mice, demonstrating hair loss and scabbing. Growth curves shown are representative of one of three independent experiments with similar results.

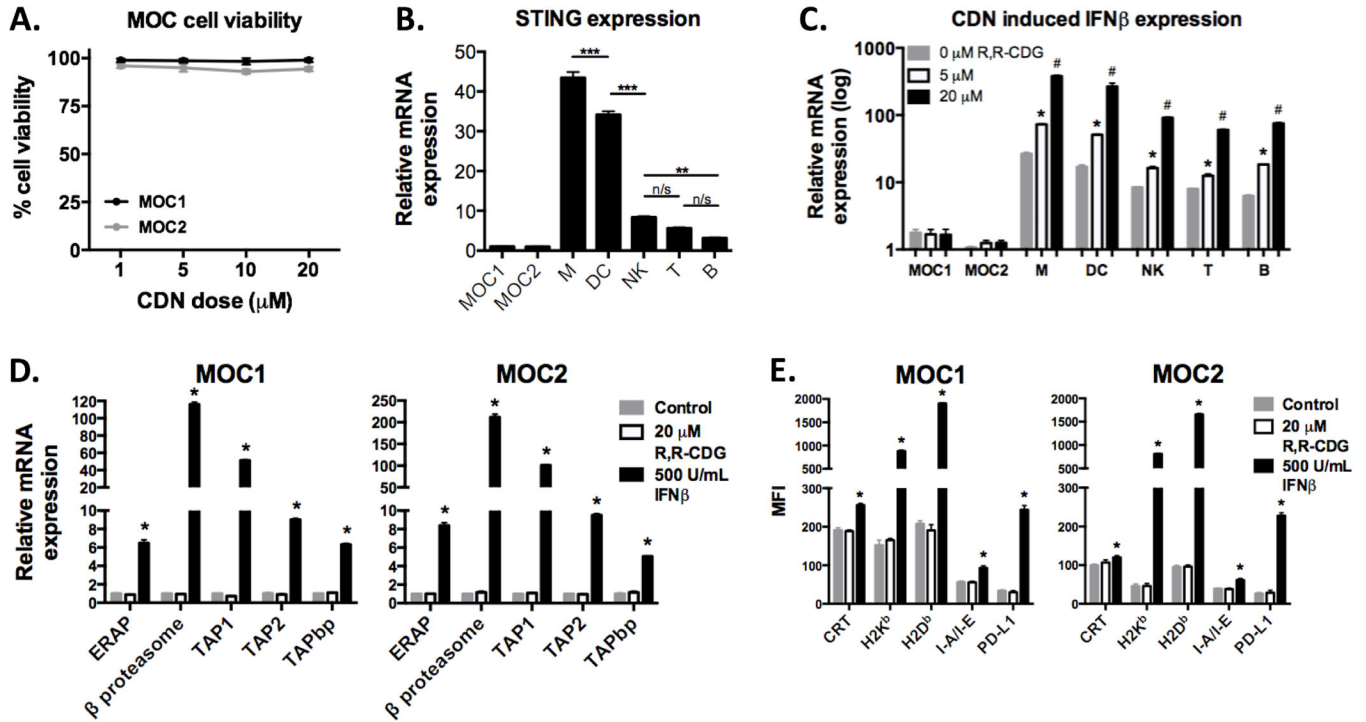


**Figure 3. Type I IFN produced following CDN activation of immune cell STING enhances immunogenicity of MOC tumor cells *in vitro***

**A**, XTT assays (48 hour time point) were used to assess MOC1 or MOC2 cell viability following exposure of up to 20  $\mu\text{M}$  R,R-CDG. Similar results were seen for at 24 and 72 hours (data not shown). **B**, RT-PCR was used to demonstrate baseline STING expression in MOC and sorted immune cells (CD11b<sup>+</sup> myeloid cells, M; CD11c<sup>+</sup> dendritic cells, DC; NK1.1<sup>+</sup> natural killer cells, NK; CD3<sup>+</sup> T lymphocytes, T; CD19<sup>+</sup> B lymphocytes, B; from spleens and lymph nodes of WT B6 mice) with expression relative to MOC1. \*\*,  $P < 0.01$ ; \*\*\*,  $P < 0.001$ ; ANOVA. **C**, MOC or sorted immune cells were stimulated with 0, 5 or 20  $\mu\text{M}$  R,R-CDG for 12 hours and quantification of IFN $\beta$  transcripts were determined relative to baseline MOC1. \*,  $P < 0.05$  relative to untreated; #,  $P < 0.01$  (ANOVA) relative to untreated and 5  $\mu\text{M}$  R,R-CDG treated cells. Similar results were observed for IFN $\alpha$  production (data not shown). **D**, Expression of transcripts of antigen processing machinery components were quantified relative to untreated groups following treatment with R,R-CDG or IFN $\beta$  for 24 hours. \*,  $P < 0.01$  (ANOVA) relative to untreated and R,R-CDG treated cells. **E**, Flow cytometry was used to assessed MOC cell surface expression of calreticulin (CRT), MHC class I (H2-K<sup>b</sup> and H2-D<sup>b</sup>), MHC class II (I-A/I-E), and PD-L1 at baseline and following treatment with R,R-CDG or IFN $\beta$  for 48 hours. \*,  $P < 0.01$  (ANOVA) relative to untreated and R,R-CDG treated cells. Results shown are from at least two independent experiments, each performed in at least technical triplicate. n/s, non-significant.

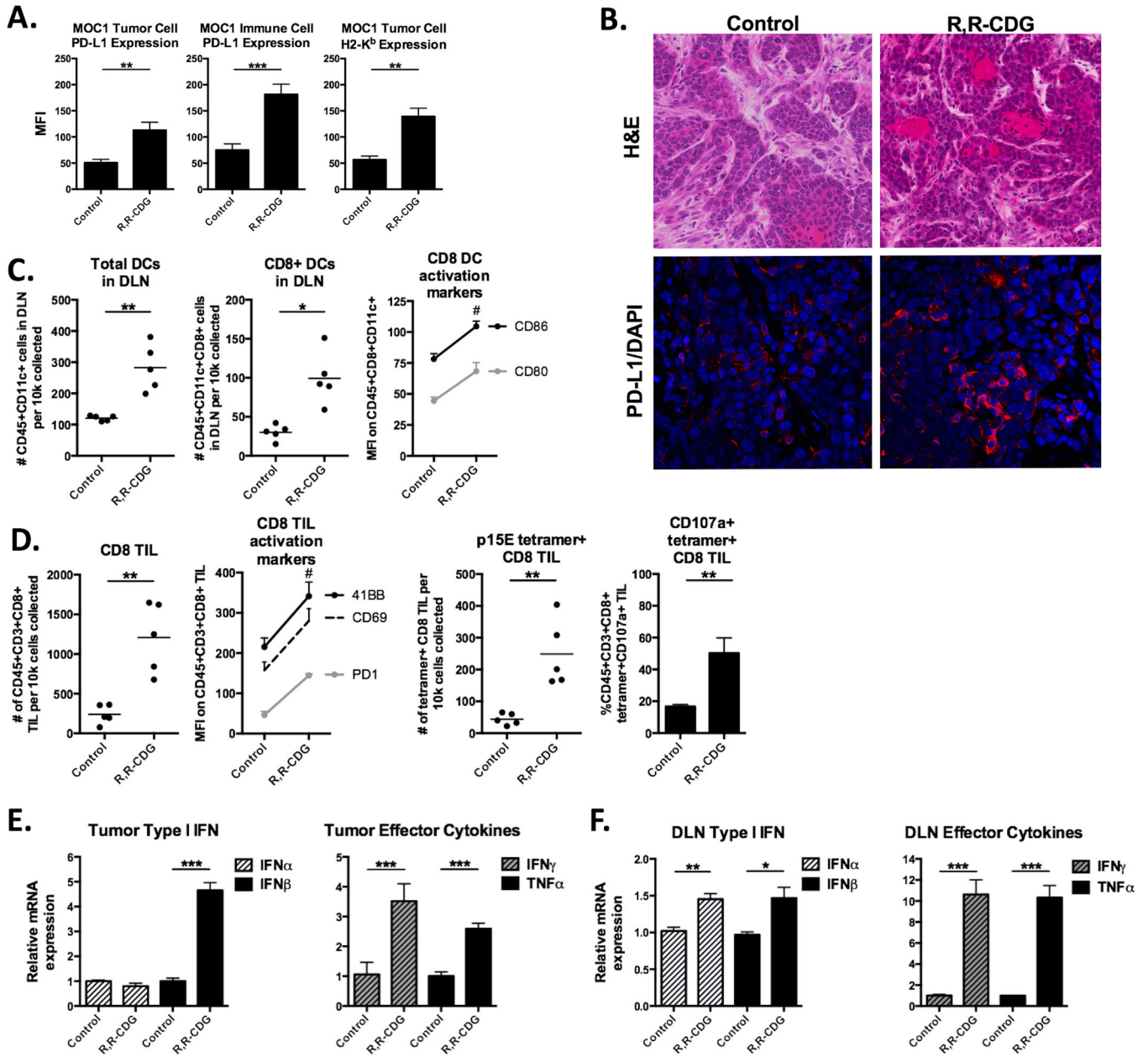


**Figure 4. CDN treated MOC1 tumors demonstrate enhanced activation of innate and antigen-specific adaptive immunity**

Tumors and tumor-draining lymph nodes (DLN) from control and R,R-CDG treated MOC1 tumor-bearing mice were harvested and analyzed by flow cytometry and immunofluorescence 48 hours after the last R,R-CDG treatment. **A**, Quantification of PD-L1 and H2-K<sup>b</sup> expression on live CD45.2<sup>-</sup>CD31<sup>-</sup> tumor cells or PD-L1 expression on live CD45.2<sup>+</sup>CD31<sup>-</sup> infiltrating immune cells from tumors following intratumoral R,R-CDG treatment (*n* = 5 mice/group). **B**, Representative H&E (top 2 panels) and immunofluorescence analysis (bottom panels) of PD-L1 (red) with DAPI counterstain (blue) in control and R,R-CDG treated tumors. 40 $\times$  magnification. **C**, Quantification of DLN total and CD8<sup>+</sup> DCs (left panels) and expression of DC activation markers (right panel) following

intratumoral R,R-CDG treatment of MOC1 tumors. #,  $P < 0.01$  for all markers. **D**, Quantification of total CD8<sup>+</sup> TILs with activation markers (left panels), and quantification of p15E<sub>604-611</sub> antigen-specific CD8<sup>+</sup> TILs (tetramer positive) and CD107a (right panels) following intratumoral R,R-CDG treatment of MOC1 tumors. Data presented as absolute number of cells per 10<sup>4</sup> live cells collected. #,  $P < 0.01$  for all markers. Whole tumor (**E**) and DLN (**F**) tissues were analyzed via RT-PCR for type I IFN (IFN $\alpha$  and IFN $\beta$ ) and effector cytokine (IFN $\gamma$  and TNF $\alpha$ ) expression following R,R-CDG treatment.  $n = 5$  mice/group. \*,  $P < 0.05$ ; \*\*,  $P < 0.01$ ; \*\*\*,  $P < 0.001$ , ANOVA.



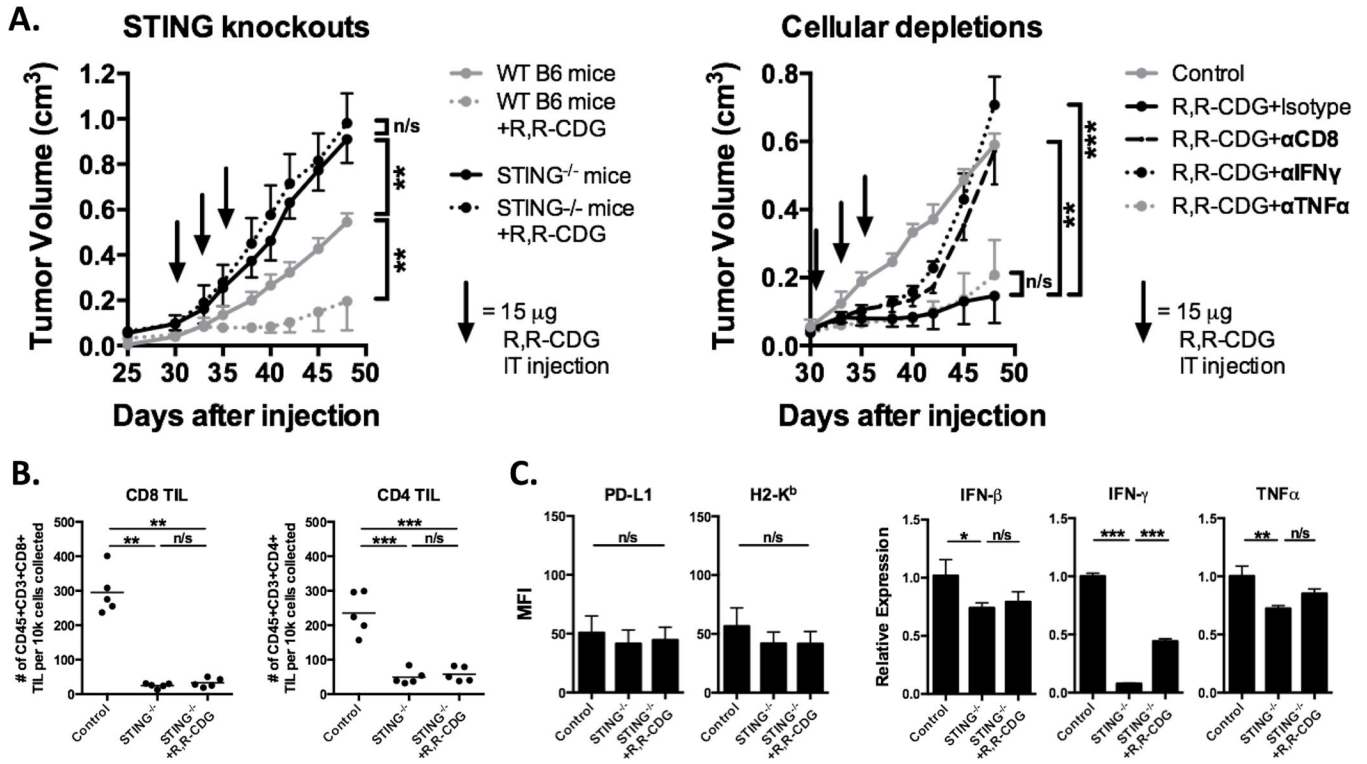


**Figure 5. Control of MOC1 tumors following CDN treatment is STING and CD8<sup>+</sup> T lymphocyte-dependent**

**A**, WT or *Tmem173<sup>gt/J</sup>* STING-deficient B6 mice were injected with  $2 \times 10^6$  MOC1 cells and established tumors were treated with intratumoral R,R-CDG (15  $\mu$ g/injection q 3 days  $\times$  3,  $n = 5-7$  mice/group, left panel). Black arrows indicate individual injections. Right panel, established MOC1 tumors were treated with intratumoral R,R-CDG (15  $\mu$ g/injection q 3 days  $\times$  3) along with systemic administration of CD8<sup>+</sup> T cell-, IFN- $\gamma$ -, or TNF $\alpha$ -depleting antibodies (200  $\mu$ g/injection IP twice weekly). Depleting antibodies were started 48 hours before R,R-CDG treatment. Control and STING-deficient mouse tissues were harvested 48 hours after the last R,R-CDG treatment and analyzed with flow cytometry and RT-PCR. **B**, quantification of CD8<sup>+</sup> and CD4<sup>+</sup> TILs in STING-deficient mice (left panels). **C**, flow cytometric quantification of PD-L1 and H2-K<sup>b</sup> on live CD45.2<sup>-</sup>CD31<sup>-</sup> tumor cells (left panels) and RT-PCR-based determination of IFN $\beta$ , IFN $\gamma$ , and TNF $\alpha$  expression relative to control (right panels,  $n = 3-5$  tumors/group). \*,  $P < 0.05$ ; \*\*,  $P < 0.01$ ; \*\*\*,  $P < 0.001$ ; ANOVA. n/s, not significant.

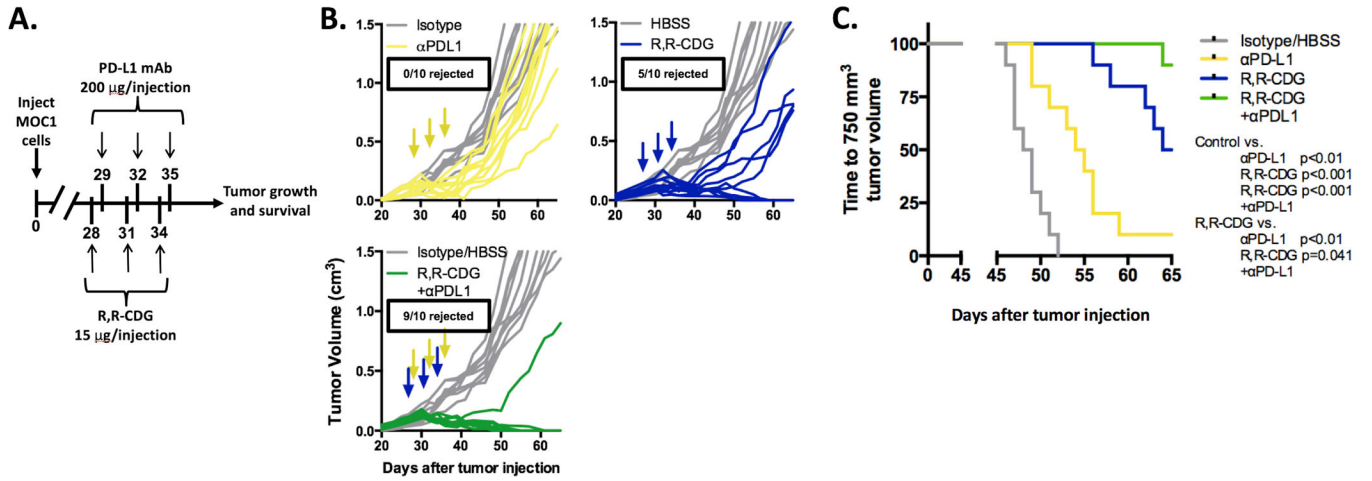


**Figure 6. Combination CDN and PD-L1 mAb treatment of established MOC1 tumors produces consistent tumor rejection**

WT B6 mice were injected with  $2 \times 10^6$  MOC1 cells and established tumors were treated with PD-L1 mAb (200 µg/injection  $\times$  3, grey arrows, control treated with rat IgG antibody) or intratumoral R,R-CDG (15 µg/injection q 3 days  $\times$  3, black arrows, controlled treated with HBSS) alone or in combination. **A**, treatment schema. **B**, individual tumor growth curves (colored) compared to control (grey). **C**, time to tumor volume of 750 mm<sup>3</sup> was assessed by log-rank/Mantel Cox analysis (significance in figure).  $n = 10$  mice/group. Results shown are representative of two independent experiments with similar results.

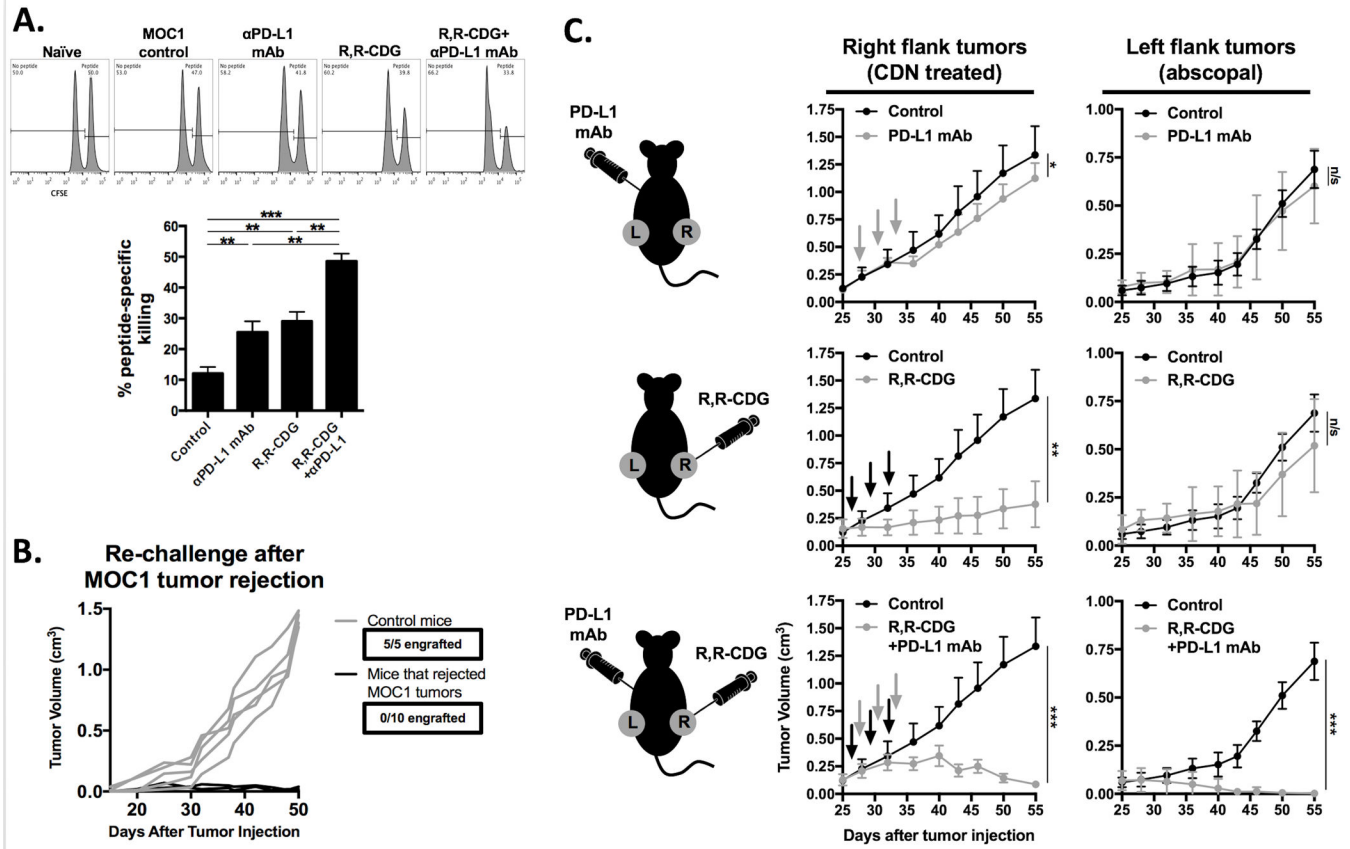


**Figure 7. Combination CDN and PD-L1 mAb treatment induces immunologic memory, protection against challenge and abscopal tumor control**  
**A,** CFSE-based *in vivo* CTL analysis using p15E<sub>604-611</sub> (KSPWF<sup>T</sup>TLL) as a model antigen ( $n = 3$  mice/group). Mice from the combination R,R-CDG and PD-L1 mAb group rejected their tumors, mice from all other groups did not reject tumors. Representative histograms from each cohort are displayed. p15E peptide-specific cell killing was quantified relative to naïve, non-tumor bearing WT B6 mice (bar graph). **B,** WT B6 mice or mice that rejected established MOC1 tumors following combination CDN and PD-L1 mAb treatment were challenged with  $2 \times 10^6$  MOC1 cells. **C,**  $2 \times 10^6$  MOC1 cells were injected bilaterally in WT B6 mice. Once tumors were established (0.1 cm<sup>3</sup>), mice were treated with CDN (right flank tumors only) and systemic PD-L1 mAb alone or in combination ( $n = 5$  mice/group) and both right and left flank tumors were followed for tumor growth. Black arrows are R,R-CDG treatment, grey arrows are PD-L1 mAb treatment. \*,  $P < 0.05$ ; \*\*,  $P < 0.01$ ; \*\*\*,  $P < 0.001$ ; ANOVA. n/s, not significant.